Key Points:
- Evaporation was quantified in a drip-irrigated desert vineyard
- Specific focus was on spatial and temporal variations across the inter-row
- Adapted HYDRUS (2-D/3-D) model successfully simulated evaporation patterns

Correspondence to:
A. Ben-Gal,
bengal@volcani.agri.gov.il

Spatial and diurnal below canopy evaporation in a desert vineyard: Measurements and modeling

D. Kool[1,2], A. Ben-Gal[1], N. Agam[2], J. Šimůnek[3], J. L. Heitman[4], T. J. Sauer[5], and N. Lazarovitch[2]

[1]Gilat Research Center, Agricultural Research Organization, Institute of Soil, Water and Environmental Sciences, Gilat, Israel, [2]Wyler Department for Dryland Agriculture, French Associates Institute for Agriculture and Biotechnology of Drylands, Jacob Blaustein Institutes for Desert Research, Ben-Gurion University of the Negev, Sede Boqer Campus, Midreshet Ben-Gurion, Israel, [3]Department of Environmental Sciences, University of California, Riverside, California, USA, [4]Department of Soil Science, North Carolina State University, Raleigh, North Carolina, USA, [5]National Laboratory for Agriculture and the Environment, Agricultural Research Service, United States Department of Agriculture, Ames, Iowa, USA

Abstract Evaporation from the soil surface (E) can be a significant source of water loss in arid areas. In sparsely vegetated systems, E is expected to be a function of soil, climate, irrigation regime, precipitation patterns, and plant canopy development and will therefore change dynamically at both daily and seasonal time scales. The objectives of this research were to quantify E in an isolated, drip-irrigated vineyard in an arid environment and to simulate below canopy E using the HYDRUS (2-D/3-D) model. Specific focus was on variations of E both temporally and spatially across the inter-row. Continuous above canopy measurements, made in a commercial vineyard, included evapotranspiration, solar radiation, air temperature and humidity, and wind speed and direction. Short-term intensive measurements below the canopy included actual and potential E and solar radiation along transects between adjacent vine-rows. Potential and actual E below the canopy were highly variable, both diurnally and with distance from the vine-row, as a result of shading and distinct wetted areas typical to drip irrigation. While the magnitude of actual E was mostly determined by soil water content, diurnal patterns depended strongly on position relative to the vine-row due to variable shading patterns. HYDRUS (2-D/3-D) successfully simulated the magnitude, diurnal patterns, and spatial distribution of E, including expected deviations as a result of variability in soil saturated hydraulic conductivity.

1. Introduction

About half of the Earth's land surface is currently considered water limited, and rising food demand is expected to continue to increase pressure on water resources [*Yermiyahu et al.*, 2007]. In water-limited environments, where evapotranspiration (*ET*) typically accounts for >95% of the water budget [*Wilcox et al.*, 2003], evaporation from the soil surface (*E*) can be a substantial source of water loss. Studies on *ET* partitioning report that, for a range of different cover types, *E* accounts for 20–40% of *ET* on average [*Kool et al.*, 2014]. In addition to concerns over diminishing water resources, the dynamics of *E* versus transpiration (*T*) also play an important role in climate processes through moisture, CO_2, and energy exchange with the atmosphere [*Scott et al.*, 2006; *Lawrence et al.*, 2007]. Accurate understanding of *E* relative to *T* is therefore critical to better identify productive and unproductive allocation of water as well as associated effects on climate and climate change [*Newman et al.*, 2006; *Peñuelas et al.*, 2009].

While the dynamics of *E* have been studied extensively for bare soils, quantification of *E* in vegetated systems remains challenging [*Kustas and Agam*, 2014; *Kool et al.*, 2014]. The presence of plants alters the microclimate and changes soil water status due to root water uptake [*Kumar et al.*, 2013, 2014]. In row-crops and orchards, *E* differs depending on row orientation, row width, plant size and architecture, and water application as a result of under-canopy wind patterns [*Heilman et al.*, 1994; *Cammalleri et al.*, 2010], shade effects [*Horton et al.*, 1984; *Horton*, 1989; *Ham and Kluitenberg*, 1993; *Colaizzi et al.*, 2010; *Pieri*, 2010], and soil water distribution across the inter-row [*Agam et al.*, 2012]. Furthermore, the magnitude of *E* relative to *ET* varies daily and seasonally depending on soil-plant interactions [*Massman and Ham*, 1994; *Newman et al.*, 2006].

Drip-irrigated wine vineyards in desert areas are high value cropping systems that warrant separate assessment of *E* [*Yunusa et al.*, 2004; *Basile et al.*, 2012; *Ortega-Farías et al.*, 2012]. Surplus water in vineyards can

cause unnecessary or excessive vegetative growth, increased disease pressure, and low grape quality [*Netzer et al.*, 2009]. Therefore, while grape production in desert areas is not feasible without irrigation, optimal water application is essential both to conserve resources and to enhance fruit quality [*Yunusa et al.*, 2004; *Basile et al.*, 2012]. Reported fractions of *E/ET* in drip-irrigated vineyards vary widely, ranging from 0.13 [*Ferreira et al.*, 2012] to 0.41 [*Yunusa et al.*, 2004], and little is known concerning the spatial or diurnal variability below the canopy that affect *ET* partitioning. Since bare soil makes up the largest part of the vineyard surface area due to wide row spacing and vine training practices, the soil surface has a relatively large contribution to the energy and water balances [*Ham et al.*, 1991; *Heilman et al.*, 1994]. Detailed information regarding *E* can support management decisions to improve water productivity and optimize vine growth [*Ferreira et al.*, 2012].

Numerical models are ideally suited to study the importance of, and interaction among, the various transient variables that determine *E*. HYDRUS (2-D/3-D) [*Šimůnek et al.*, 2008] is a widely used numerical model simulating water flow in the soil, which has been previously used to study components of *ET* in, for example, cotton [*Bufon et al.*, 2012] and pecans [*Deb et al.*, 2013]. However, the model has never been validated for accurate partitioning between *E* and *T*. Similar to other drip-irrigated row crops and orchards, the main variables determining *E* in a drip-irrigated vineyard are expected to be soil water content and atmospheric boundary conditions, which are subject to shading and therefore not uniform across the inter-row. HYDRUS (2-D/3-D) has been found to successfully simulate wetting patterns under drip irrigation [*Skaggs et al.*, 2004; *Lazarovitch et al.*, 2009; *Hinnell et al.*, 2010] but requires adaptation to incorporate and allow for spatial variability in boundary conditions at the soil surface. The objectives of this study were to quantify *E* in an isolated, drip-irrigated vineyard in an arid environment and to employ HYDRUS (2-D/3-D) to simulate below canopy *E* while considering variability in time and space.

2. Methods

2.1. Site Description
An experiment was conducted in a commercial vineyard under drip irrigation, located in Israel's arid central Negev highlands (30.7°N, 34.8°E). Long-term temperature averages range from 4.4 to 14.8°C in January and 18.1 to 32.7°C in July. Average annual precipitation is <100 mm, falling erratically between November and April (Israel meteorological service). The 10 year old Cabernet Sauvignon (*Vitis vinifera* L.) vineyard formed an isolated irrigated area in a dry bare surrounding with field dimensions of approximately 430 × 230 m (~10 ha) in the north-south and east-west directions, respectively. Row orientation was approximately north-south. The vines were planted 1.5 m apart, with 3 m spacing between rows, and were trained on a vertical-shoot-positioned system, with 1 m cordon height. At full maturity, the canopy was 2 m high with 17% of the total soil surface area shaded beneath the canopy at solar noon.

2.2. Experimental Setup
A micrometeorological station was located at the south-east side of the vineyard with a fetch ranging from 200 to 500 m depending on the instantaneous wind direction. The prevailing wind direction at the site is north-west. Data were collected continuously as part of a larger experiment that spanned over the 2011–2012 growing seasons. Standard meteorological measurements above the canopy included wind speed and direction (Wind Sentry, R.M. Young, Traverse City, MI), air temperature and relative humidity (HMP45C, Vaisala Inc., Woburn, MA and 10-Plate Gill Radiation Shield, R.M. Young, Traverse City, MI), solar radiation (LI-200SA Pyranometer, Li-Cor Biosciences, Lincoln, NE), and precipitation (TE525 tipping bucket rain gage, Texas Electronics Inc., Dallas, TX). A water meter (WMR, Arad Ltd., Dalia, Israel) was used to monitor irrigation events. As part of the energy budget, net radiation was measured at 5 m height (Q*7, Radiation and Energy Balance Systems, Seattle, WA). Soil heat flux was computed as a weighted average of measurements at five positions across the inter-row, using five flux plates (HFT1.1, Radiation and Energy Balance Systems, Seattle, WA) at 0.06 m depth, and accounting for heat storage using thermocouples at depths of 0, 0.015, 0.045, and 0.06 m adjacent to each plate [*Sauer*, 2002]. Data were logged at 10 s intervals, and 15 min averages were stored using CR23X and CR5000 data loggers (Campbell Scientific Inc., Logan, UT). In addition, hourly wind speed, temperature, and humidity, at 2 m height, were retrieved from a weather station located 1 km to the north of the experimental site, in order to compute reference *ET* (*ET*$_0$) according to the FAO Penman-Monteith model [see details in section 2.3.2, *Allen et al.*, 1998].
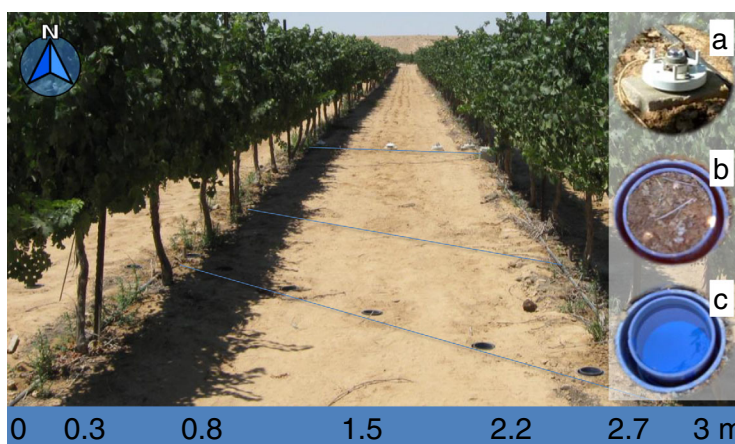
Figure 1. Below canopy measurement setup for intensive observation periods (a) with a row of pyranometers in the back, (b) a row of microlysimeters, and (c) a row of micropans in front.

Vineyard *ET* and sensible heat fluxes were determined using an eddy covariance system (CSAT 3-D sonic anemometer, Campbell Scientific Inc., Logan, UT; with an open path infrared gas analyzer, LI-7500, Li-Cor Biosciences Inc., Lincoln, NE) mounted 2 m above the plant canopy, facing north-west. Data were recorded at 10 Hz using a CR5000 data logger (Campbell Scientific Inc., Logan, UT). Postprocessing of the eddy covariance data included despiking according to the algorithm developed by *Goring and Nikora* [2002], correction for humidity and crosswind effects on sonic temperature [*Schotanus et al.*, 1983; *Liu et al.*, 2001], 2-D coordinate rotation correction [*Tanner and Thurtell*, 1969], frequency response correction [*Massman*, 2000], and the correction for buoyancy effects described by *Webb et al.* [1980].

Below canopy measurements were conducted at six positions across the inter-row (Figure 1) during two intensive observation periods (IOPs) toward the end of the season when the canopy was fully developed (3–5 and 22–24 July 2012). Below canopy *E* was measured using microlysimeters (MLs). The MLs were 100 mm deep with a diameter of 110 mm and were made of PVC to minimize heat conduction away from the surface [*Evett et al.*, 1995]. Undisturbed soil cores were kept in the field for less than 48 h to maintain realistic bottom boundary conditions [*Boast and Robertson*, 1982] following the procedure described by *Agam et al.* [2012]. As MLs cannot be used during or immediately after irrigation due to changing boundary conditions, measurements could only be taken on days following an irrigation event. Since irrigation was applied every other day, ML measurements were only conducted for 1 day during each IOP. The MLs were pushed into the soil, excavated, capped to prevent losses other than evaporation, weighed and placed in a preformed hole with the same position relative to the vine-row as the original sample location. The installed MLs were removed and weighed hourly from predawn to after sunset. The scale's resolution was 0.1 g, which corresponded to 0.011 mm. Two replicates for each position, with a total of 12 MLs, were sampled during IOP1. Because of the high variability in *E* observed at the position directly under the vine during IOP1, the ML setup for IOP2 was adjusted to one replicate for positions 0.8, 1.5, and 2.2 m, two replicates for positions 0.3 and 2.7 m, and six replicates for the position directly underneath the vine. The MLs directly under the vine represented distinctly wet and distinctly dry areas (each with three MLs). Variations in atmospheric conditions across the inter-row were investigated by measuring solar radiation (R_s) using pyranometers (CMP3, Kipp & Zonen, Delft, Netherlands) and potential *E* using micropans. The micropans were designed similar to the MLs except that the cylinder was filled with water. A reference micropan was installed in an open nonshaded area in the vineyard. Pyranometer data were logged at 10 s intervals, and 15 min averages were stored using a CR10 data logger (Campbell Scientific Inc., Logan, UT). The micropans were weighed hourly at a resolution of 0.05 g, corresponding to 0.006 mm, with two replicates for each position. Thermal images were acquired hourly using a thermal camera (FLIR T335, FLIR Systems Inc., USA).

2.3. Modeling
2.3.1. Model Adaptation
The HYDRUS (2-D/3-D) model numerically computes evaporation and infiltration fluxes across the surface interface where the flux is limited either by a predefined potential flux or by the soil moisture

conditions [*Šimůnek et al.*, 2008]. In its two-dimensional form, the surface boundary condition is given as follows:

$$\left| K \left(K_{ij}^A \frac{\partial h}{\partial x_j} + K_{iz}^A \right) n_i \right| \leq E_{pot} \tag{1}$$

and

$$h_A \leq h \leq h_s \tag{2}$$

where K is the unsaturated hydraulic conductivity (m/h), K_{ij}^A are components of a dimensionless anisotropy tensor K^A, h is the soil surface pressure head (m), x_i ($i = 1, 2$) are the spatial coordinates (x, z) in (m), n_i are components of the outward unit vector normal to surface boundary, E_{pot} is the maximum or potential rate of either infiltration or evaporation based on atmospheric conditions (m/h), and h_A and h_S are the lower and upper limits for h, respectively. The value of h_A can be determined from the equilibrium conditions between soil water and atmospheric water vapor pressure, whereas h_S is generally set to zero, assuming there is no surface ponding.

The standard version of HYDRUS (2-D/3-D) calculates actual E from E_{pot} and soil moisture status for boundaries with an "Atmospheric" boundary condition (BC), for which potential fluxes of precipitation and evaporation have to be specified. The standard version of HYDRUS (2-D/3-D) also allows one "Time-Variable Flux" BC to be treated as an atmospheric BC, i.e., with limited pressure heads (equation (2)). For this study, in which E_{pot} was variable across the soil surface, HYDRUS (2-D/3-D) was modified so that it could treat up to four different Time-Variable Flux BCs as Atmospheric BCs, i.e., with actual fluxes limited by the soil moisture conditions.

Water distribution in a drip-irrigated system can be considered either radially symmetrical around a dripper, fully three-dimensional [*Kandelous et al.*, 2011], or essentially two-dimensional due to close spacing and overlapping of wetting from adjacent emitters. Concurrently, E_{pot} at the soil surface is predominantly two-dimensional, varying along the cross section between two rows. For simplification purposes, the drip laterals were assumed to be line sources, thus allowing two-dimensional modeling. Hourly measurements of E acquired during the IOPs were used to calibrate (first IOP, 3–5 July) and validate (second IOP, 23–25 July) the simulated fluxes. Initial water profile conditions of the domain were obtained by running presimulation over a 3 month period before bud-break, using ET_0 data as an atmospheric BC and zero root water uptake. Total simulation time was 2784 h, from bud-break on 1 April until a week before harvest on 25 July.

2.3.2. Reference Evapotranspiration
Hourly reference ET (ET_0) was used to estimate both potential transpiration (T_{pot}, section 2.3.5) and E_{pot} (section 2.3.6). The FAO Penman-Monteith equation for hourly time steps is [*Allen et al.*, 1998]:

$$ET_0 = \frac{0.408\Delta(R_n - G) + \gamma \frac{37}{T_h + 273} u(e_s - e_a)}{\Delta + \gamma(1 + 0.34u)} \tag{3}$$

where ET_0 is the ET rate (mm/h) from a well-watered reference surface, R_n is net radiation at the reference surface (MJ/m^2/h), G is soil heat flux density (MJ/m^2/h), T_h is mean hourly temperature (°C), Δ is the saturation slope vapor pressure curve at T_h (kPa/°C), γ is the psychrometric constant (0.067 kPa/°C), e_s is the saturated vapor pressure at T_h (kPa), e_a is the average hourly actual vapor pressure (kPa), and u is average hourly wind speed (m/s). The calculations were conducted according to the recommended procedure based on data of T_h, u, relative humidity (RH), and R_s from a nearby weather station. The reference surface is a hypothetical green grass to which other surfaces can be related, thus expressing climate parameters independent from soil and plant characteristics. As the weather station represented arid conditions rather than well-watered conditions, computed ET_0 underestimated real ET_0. However, ET_0 was not adjusted to better represent well-watered conditions, as the nonadjusted ET_0 was expected to best characterize the natural evaporation demand of the climate [*Allen et al.*, 1998; *Temesgen et al.*, 1999].

2.3.3. Domain Parameters
The flow domain (Figure 2) was chosen to represent a cross section from midrow to midrow, with time and space-variable atmospheric boundary conditions (Neumann type) at the soil surface, zero flux on the sides of the domain and free drainage at the bottom of the profile. The domain was discretized into 12,772
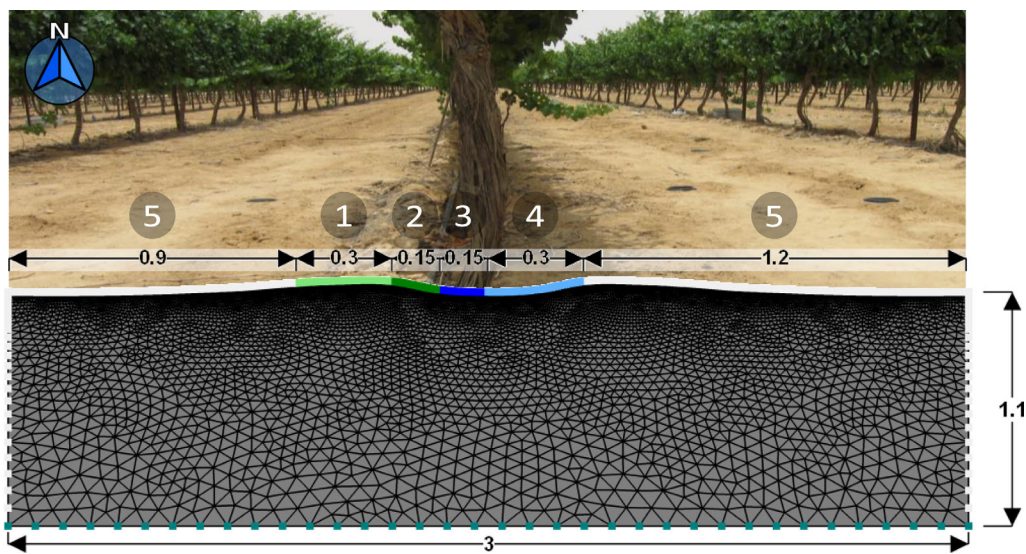
Figure 2. Variable boundary conditions simulated in HYDRUS (2-D/3-D) with (1) potential flux for position 2.7 m (A), (2) potential flux A + irrigation, (3) potential flux for position 0 m (B) + irrigation, (4) potential flux B, and (5) no flux; and free drainage at the bottom of the profile. Dimensions are in meters.

triangular finite elements (6581 nodes) using an unstructured finite element mesh, with a finer mesh close to the surface [*Warrick and Lazarovitch*, 2007]. The roots were located throughout the complete depth over a 1 m cross section below the vine location, with a uniform relative distribution function of 0.45 in the top 0.4 m, and a linear decline to 0 toward the bottom of the profile. Soil surface Areas 1 and 2 represent inter-row position 2.7 m (Figure 1), where Area 2 falls within the wetted area of the dripper and Area 1 does not. Similarly, Areas 3 and 4 represent inter-row position 0 m (Figure 1), with Area 3 within the wetted area of the dripper, and Area 4 outside the wetted area. Area 5 represents the midrow positions where E was assumed to be zero.

2.3.4. Hydraulic Parameters
Soil hydraulic parameters of the van Genuchten-Mualem functions [*Mualem*, 1976; *van Genuchten*, 1980] were estimated based on soil texture and bulk density measurements, using neural network predictions with the ROSETTA package [*Schaap et al.*, 2001; Table 1]. Analysis of the effects of spatial variability in soil hydraulic conductivity was obtained by generating 40 realizations with a lognormal distribution of saturated hydraulic conductivity (K_s) using a scaling factor (y) where the standard deviation of log 10(y) was 0.5, and correlation lengths $x = 0.05$ m and $z = 0.05$ m, respectively, following *Lazarovitch et al.* [2006].

2.3.5. Root Water Uptake Parameters
Root water uptake was simulated according to the water stress response function suggested by *Feddes et al.* [1978]. The water stress response function was extended following *Jarvis* [1989] with a critical stress index (ω_{crt}) [*Šimůnek and Hopmans*, 2009] to balance reduced water uptake from one part of the root zone by increased uptake from a less stressed region of the root zone. The ω_{crt} factor allows for water uptake compensation proportional to the water stress response function, where $\omega_{crt} = 1$ is noncompensated uptake and compensation increases as ω_{crt} approaches zero. Visual observations of root distribution along

Table 1. Soil Texture and Hydraulic Properties[a]

Particle Size Distribution[b] (%)									
Sand	Silt	Clay	Soil Texture[b]	ρ_b[b] (kg m^{-3})	θ_s (m^3 m^{-3})-	θ_r (m^3 m^{-3})-	α (m^{-1})	n	K_s (m h^{-1})
53.4	20.3	26.3	Sandy clay loam	1400	0.43	0.07	1.8	1.4	0.02

[a]ρ_b, soil bulk density; θ_s, saturated volumetric water content; θ_r, residual water content; α and n, empirical shape parameters; and K_s, saturated hydraulic conductivity.
[b]Measured values.

Table 2. Root Water Uptake Parameters[a]

Optimization	ω_{crt}	h_3 (m)
Min	0.1	−30
Max	0.9	−120
Δ	0.05	10
N	17	10
Final value	0.3	−50

[a]Where h_3 is the pressure head below which root water uptake ceases, associated with the water stress response function [*Feddes et al.*, 1978], and ω_{crt} is the critical stress index [*Jarvis*, 1989]. The optimum values were found by running *N* simulation between *Min* and *Max* values over Δ intervals for respective parameters.

the face of an exposed profile indicated that virtually all roots were located within a 0.5 m radius from the drip line. In the absence of root measurements, root water uptake parameters were obtained from the literature and by optimization. Feddes parameter h_1, the pressure head below which roots extract water at the maximum possible rate, was set to −0.5 m. The pressure head below which root water uptake starts to decline, h_2, was set to −10 m, according to values reported for mature wine vineyards [*Taylor and Ashcroft*, 1972]. Since root water uptake indirectly determines evaporation through water availability, root parameters, h_3 and ω_{crt} (Table 2), were chosen to optimize agreement between the measured and simulated results for hourly *E* during the calibration IOP. Potential transpiration (T_{pot}) was estimated hourly using the FAO-56 dual K_c procedure, where ET_0 is multiplied by a crop-specific factor (K_{cb}). Late season K_{cb} was estimated according to the shade-K_{cb} model [*Williams and Ayars*, 2005], where the fraction shaded area at noon is considered the ground cover fraction (GCF). The K_{cb} can be estimated as $K_{cb} = \sim[0.02 \times GCF + 0.07]$ following two independent studies for six different vineyards, assessing five different wine cultivars [*Ferreira et al.*, 2012; *Picón-Toro et al.*, 2012]. The K_{cb} was set to increase linearly until reaching a constant maximum value (the late season K_{cb}) for the last 40 days of the season.

2.3.6. Boundary Conditions
The minimum allowed *h* at the surface (h_A) was set to −150 m, a default value in HYDRUS (2-D/3-D). This value is much higher than expected h_A under desert conditions, however, sensitivity analysis to h_A revealed marginal differences in *E* for $h_A < -150$ m, while computation time increased exponentially. The surface boundary was divided into five sections (Figure 2) using the adapted HYDRUS (2-D/3-D) model with the option "*Treat the time-variable flux boundary as the atmospheric boundary condition, i.e. with limited pressure heads*" applied to all time-variable fluxes. The Atmospheric BC option was used to obtain more detailed *E* outputs for Area 4. In order to retrieve a full picture of changes in *E* over the gradient from wet to dry, fluxes were calculated in adjacent 10 cm strips. Simulations were run to assess *E* between 0 and 0.1 m, 0.1 and 0.2 m, and 0.2 and 0.3 m from the wetted area (Area 3). Potential flux was set to hourly reference ET_0 calculated with below canopy R_S measured for inter-row positions 2.7 m (potential flux A) and 0 m (potential flux B), respectively (Figure 1). Irrigation events were simulated over Areas 2 and 3, using measured irrigation data divided by respective surface areas, subtracted by E_{pot}, thus forcing *E* to equal E_{pot} in the wetted areas during irrigation events.

2.3.7. Model Evaluation
Agreement between simulated and measured hourly *E* was assessed by means of the Nash-Sutcliffe efficiency (NSE) [*Nash and Sutcliffe*, 1970], and the root-mean-square errors (RMSE) [*Willmott*, 1982]:

$$NSE = 1 - \frac{\sum_{t=1}^{N}(E_{obs}(t) - E_{sim}(t))^2}{\sum_{t=1}^{N}(E_{obs}(t) - \overline{E}_{obs})^2} \tag{4}$$

$$RMSE = \left[N^{-1}\sum_{t=1}^{N}(E_{obs}(t) - E_{sim}(t))^2\right]^{1/2} \tag{5}$$

where *N* is the number of observations, *t* is time (h), and subscripts "obs" and "sim" refer to observed and simulated *E* (mm/h), respectively. The model was optimized to obtain the largest NSE and lowest RMSE for measured and simulated average *E* directly underneath the vine (Areas 3 and 4, Figure 2) for the calibration IOP. Resulting NSE and RSME of *E* from the second IOP were used for validation.

3. Results

3.1. Field Conditions
Total precipitation at the vineyard from November 2011 to March 2012 (the rainy season prior to the 2012 growing season) was 48.3 mm. The last rainfall event (2.5 mm) occurred on 16 March. The growing season
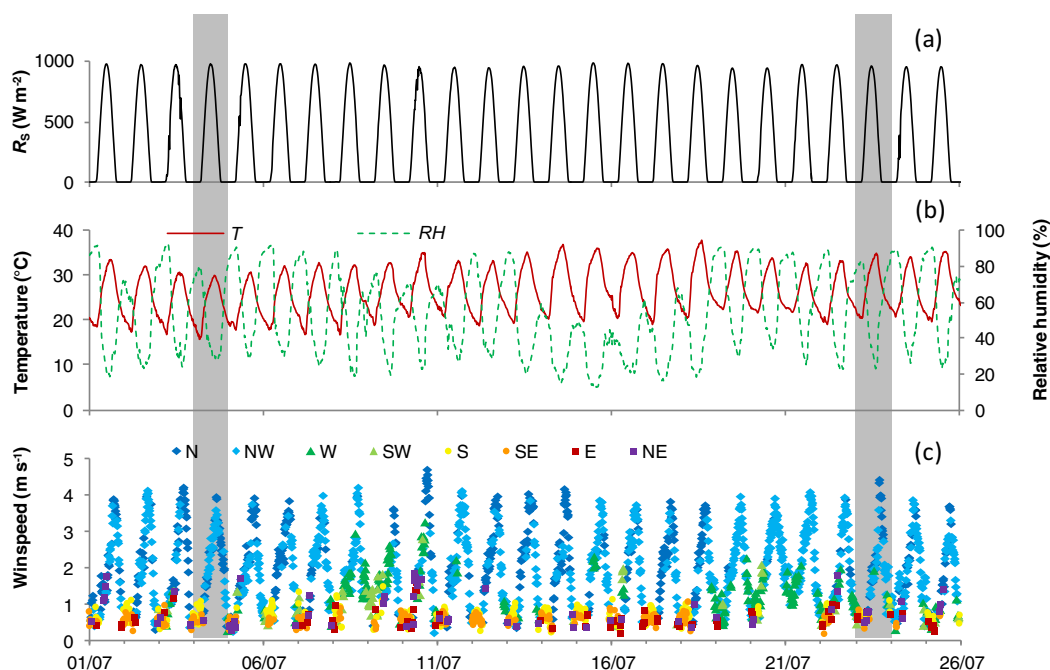
Figure 3. Field conditions for 1–25 July 2012. (a) Solar radiation (R_S). (b) Temperature (T) and relative humidity (RH) at 3 m height. (c) Wind speed at 3 m height; symbols and colors represent different wind directions: north (N), northwest (NW), west (W), southwest (SW), south (S), southeast (SE), east (E), and northeast (NE). Days that were used for calibration and validation of the model are marked by gray bars.

started with bud-break on 1 April and data were collected until 26 July, shortly before harvest. No precipitation occurred during the growing season. Analysis of below canopy E is reported for the month of July, during which the canopy was fully developed. This period coincided with veraison in the vineyard. The atmospheric conditions in July were characterized by clear days with little variation from day to day (Figure 3). Generally, there were no clouds, resulting in a very regular pattern of R_S (Figure 3a). Air temperature fluctuated between about 35°C during the day and 20°C at night, and relative humidity between 25% and 90%, respectively (Figure 3b). Wind direction was predominantly northwest and wind speeds tended to increase during the day, typically reaching a peak of about 4 m/s between 16:30 and 17:00 in the afternoon (Figure 3c).

Similar to the atmospheric conditions, ET_0 followed a regular diurnal pattern averaging 7.3 mm/d (Figure 4) with average peak values of 0.79 mm/h. Irrigation was applied three times a week at 2 or 3 day intervals with an average application of 7.5 mm per event. Average ET amounted to 3.08 mm/d, with average peak values of 0.43 mm/h, and was strongly affected by irrigation events (Figure 4). On days immediately following irrigation, ET reached highs of up to 0.61 mm/h, dropping to lows of 0.21 mm/h on the second day without irrigation.

3.2. Below Canopy Conditions
3.2.1. Shade and Temperature Patterns
Distinct diurnal patterns of shaded and sunlit soil surface, dependent on solar position and vineyard architecture, are illustrated in Figure 5. A thermal image acquired at 12:35 on 23 July 2012 (Figure 6) shows large heterogeneity in soil surface temperature; which is an indicator both of soil water status and available energy at the soil surface. The soil surface temperature is expected to be inversely related to the evaporation rate. At the time of acquisition, the central part of the inter-row was sunlit, and temperatures exceeded 60°C in the center (red tints in Figure 6) with temperatures of about 45°C (yellow tints) in the area where shade had just receded. Below the vine, distinct wet (~28°C) and dry (~34°C) areas could be observed.

3.2.2. Below Canopy Radiation and Evaporation
Diurnal below canopy radiation (R_{S_below}) and micropan evaporation (E_{pot_below}) resembled the patterns of soil surface shading under the canopy (Figure 7). The reduction in R_{S_below}, compared to the above canopy R_S (R_{S_ref}), was as great as 90% during periods of shading, while E_{pot_below} decreased by about 50%
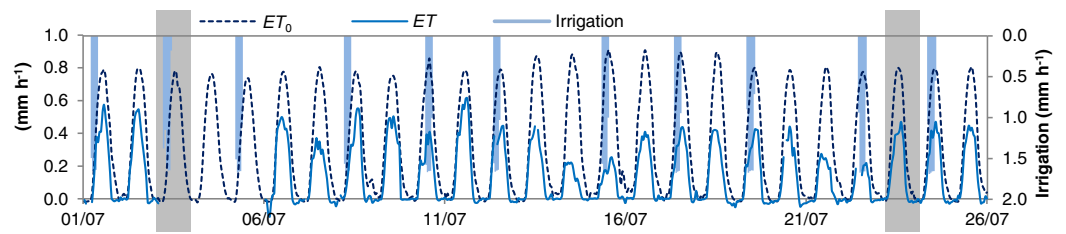
Figure 4. Hourly fluxes for 1–25 July 2012. Evapotranspiration (ET) is driven by reference ET (ET_0) and irrigation.

Figure 5. Hourly changes in shade patterns across the inter-row, facing north.

compared to that measured outside the vineyard (E_{pot_ref}). The position directly underneath the vine experienced the greatest reduction in both R_{S_below} and E_{pot_below}, as shading occurred around solar noon, the time of peak radiation. Cumulative daily E_{pot_below} ranged from 6.5 to 8.0 mm across positions for 4 July and from 7.0 to 8.9 mm for 23 July. Evaporative demand was about 20% lower at the below vine position
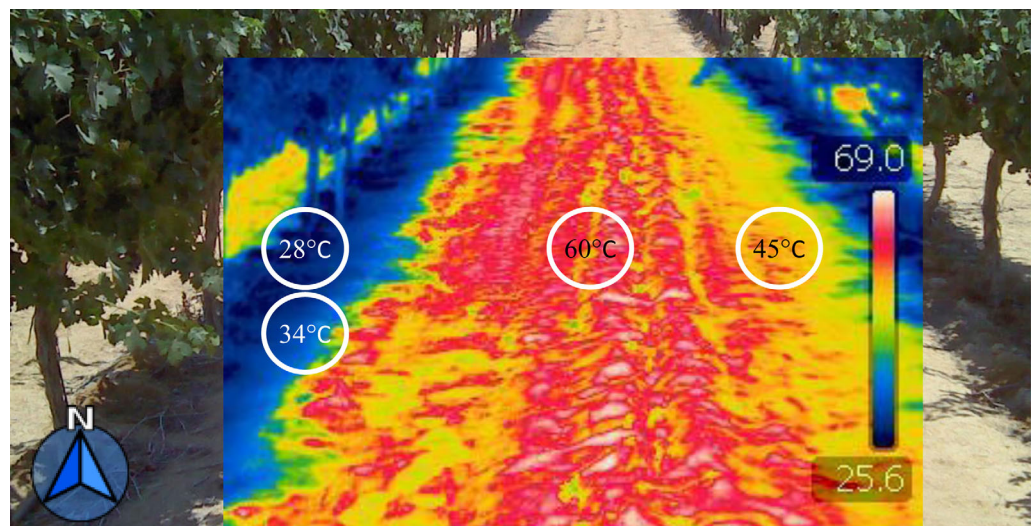

Figure 6. RGB image with overlaid thermal image of the vineyard inter-row that were acquired simultaneously on 23 July 2012 at 12:35. The legend refers to temperature (°C) and circled numbers represent average temperatures for respective surfaces.
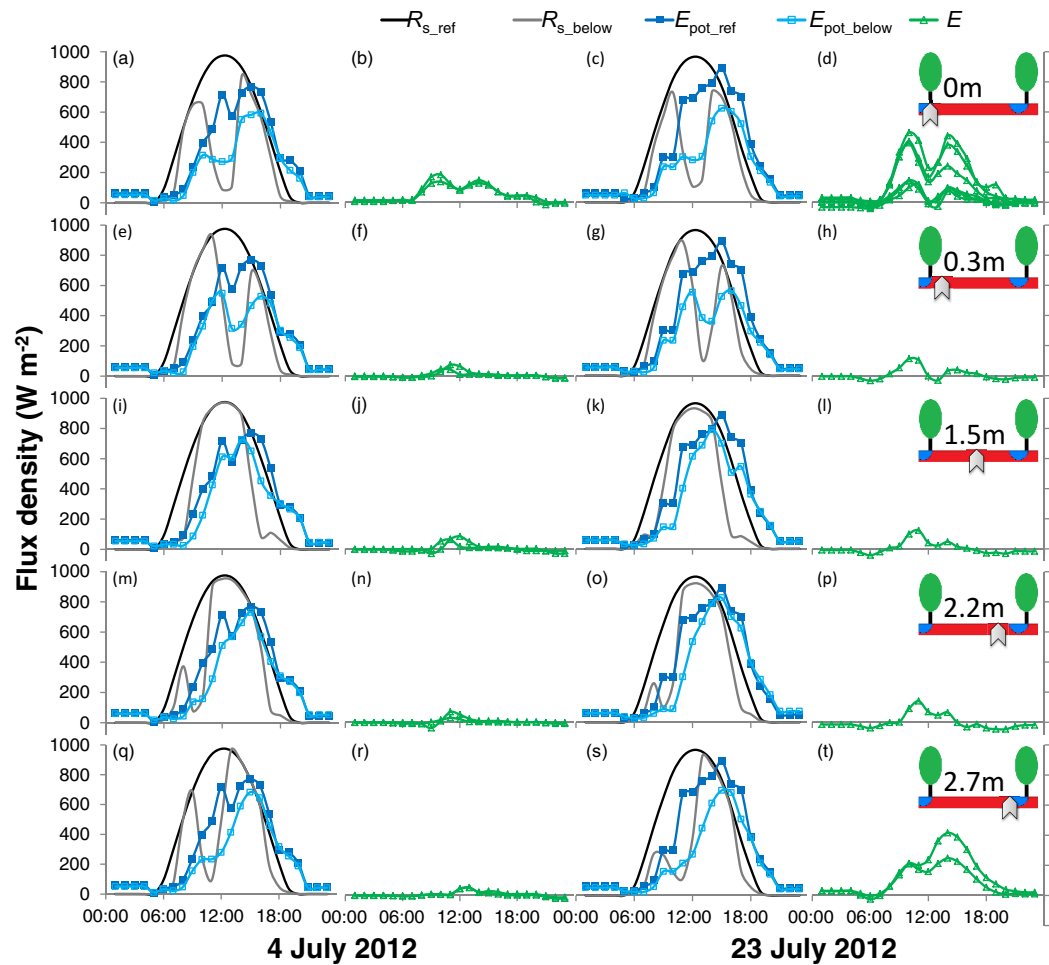
Figure 7. Hourly changes in radiation and actual and potential evaporation fluxes from reference measurements and for five positions across the inter-row: (a–d) 0 m, (e–h) 0.3 m, (i–l) 1.5 m, (m–p) 2.2 m, and (q–t) 2.7 m for 4 and 23 July 2012. RS_ref is solar radiation above the canopy, RS_below is solar radiation at the respective position below canopy, Epot_ref is potential evaporation outside the vine-row, Epot_below is potential evaporation below the canopy, and E is actual evaporation below the canopy where each line represents one microlysimeter.

compared to the midrow position. The diurnal patterns of E were similar to E_{pot_below}, but less pronounced, and both E and E_{pot_below} lagged behind R_{S_below}. Actual E was concentrated mostly in positions 0 and 2.7 m, close to the location of the dripper (∼2.9 m). On 4 July, cumulative E directly underneath the vine equaled 2 mm according to MLs located at random distances from the drippers. On 23 July, MLs were located at distinct dry and wet areas below the vine (position 0, with "wet" MLs deployed immediately under a dripper and "dry" MLs 0.25 m from the dripper; distance between drippers was 0.5 m). Average cumulative E amounted to 0.7 and 4 mm/d for the dry and wet MLs, respectively. The daily sums for positions 0.3–2.2 m were negligible. Overall daily E was about 0.26 mm on 4 July and 0.52 mm on 23 July,
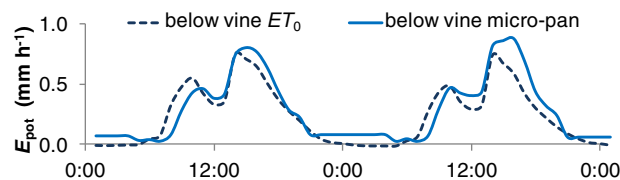
assuming positions 2.7 and 0 m each represented 0.3 m of the inter-row and that the remaining 2.4 m did not contribute to E fluxes.

3.3. Modeling Results
3.3.1. Model Parameterization
Optimization of root water uptake parameters ω_{crt} and h_3 (Table 2) was limited to evaporation data from the position directly underneath the vine (Areas 3 and

Figure 8. Estimated potential evaporation (Epot) with reference evapotranspiration ($ET0$) using below canopy radiation and micropan evaporation for 4–5 July 2012.
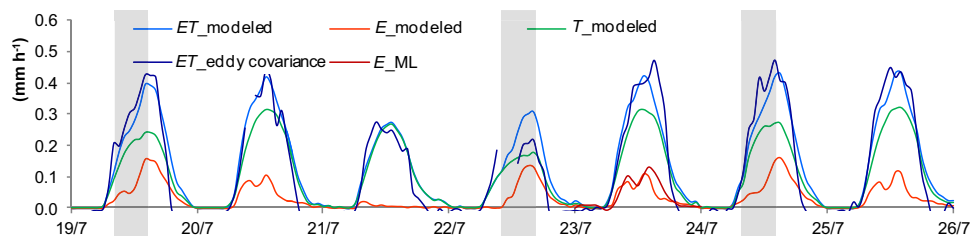
Figure 9. Evapotranspiration (*ET*), transpiration (*T*), and evaporation (*E*) fluxes, where (_modeled) are fluxes simulated using HYDRUS (2-D/3-D) and (_ML) and (_eddy covariance) are microlysimeter and eddy covariance measurements, respectively. Gray bars indicate irrigation periods.

4, Figure 2). The optimized values resulted in an NSE of 0.44 and a RMSE of 0.06 mm/h for modeled versus measured hourly *E* during the calibration IOP. Linear regression resulted in an R^2 of 0.74 with an intercept that did not differ significantly from 0 ($p > 0.05$). The results were more sensitive to ω_{crt} than to h_3 (Table 2). The K_{cb} was computed to be 0.40 for the month of July which corresponds to 17% shading of total vineyard surface area at noon (see section 2.3.5). Estimated below canopy ET_0, using below canopy radiation data, was compared to micropan data (Figure 8) to evaluate whether the method could be used as input for E_{pot} in simulations. Data comparison resulted in an R^2 of 0.86 and a slope of 1.01. The intercept was not significantly different from 0 ($p > 0.05$).

3.3.2. Evapotranspiration Partitioning
Modeling results with the optimized parameters are shown along with measurements in Figure 9. Total below canopy *E* computed by HYDRUS (2-D/3-D) was compared to an average of ML measurements weighted according to representative surface area. In addition, modeled *ET* was compared to eddy covariance measurements. An energy budget over 30 min intervals assessed for day-time data over the whole season (data not shown) indicated that eddy covariance latent and sensible heat were fairly linear with measured net radiation and soil heat flux, with an R^2 of 0.74, a slope of 1.13 and an intercept of -55 W/m^2. A stationarity test for eddy covariance *ET* indicated some uncertainty for the data between 15:00 and 9:00 the following morning. Statistical comparison was thus limited to time periods between 9:00 and 15:00. Good correlation was found between measured and modeled *ET* and *E*. Total modeled *ET* for the periods between 9:00 and 15:00 over the whole week was 96% of measured *ET* for the corresponding period. While the model slightly underestimated *ET* for most days, it overestimated *ET* on irrigated days. As a result, modeled and measured *ET* values were more similar on days following an irrigation event. Comparison of the *ET* data resulted in an NSE of 0.62, RMSE of 0.05 mm/h and an R^2 of 0.65, with a slope of 1.04 and an intercept of 0 mm/h. The results for *E* gave an NSE of 0.73, RMSE of 0.02 mm/h and an R^2 of 0.76, with a slope of 0.69 and an intercept of 0.01 mm/h. The cumulative modeled *E* for 23 July was about 20% less than measured *E*.
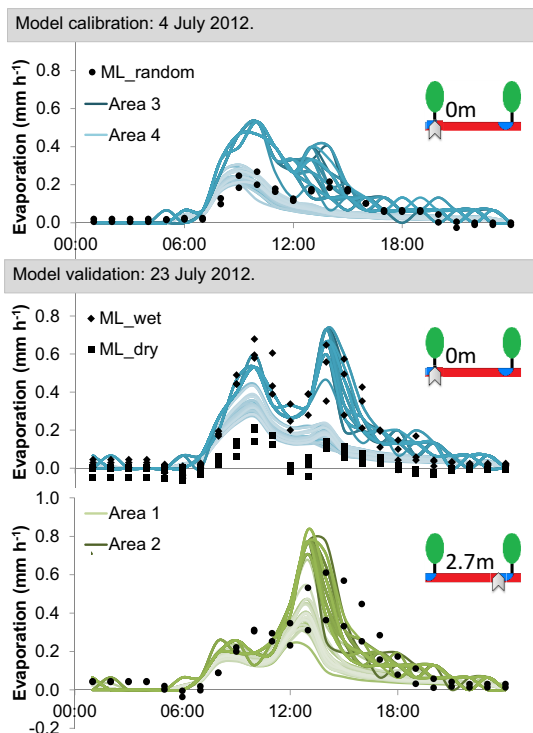

Figure 10. Model calibration and validation for 40 simulations, where each simulation had a different random distribution of saturated hydraulic conductivity. Microlysimeter (ML) measurements were collected from random, wet, and dry positions across areas 1 and 2 and 3 and 4 (see Figure 2).

3.3.3. Below Canopy Variability
Individual ML measurements were plotted against results of 40 different realizations, where each simulation had a different randomized soil
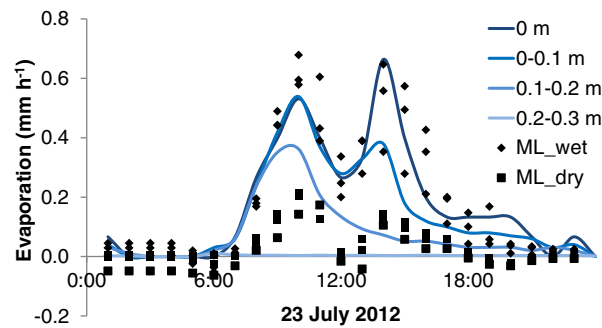
Figure 11. Simulated variability in evaporation as a function of distance from wetted area (0 m). Microlysimeter (ML) measurements were collected from distinctly wet and dry areas below the vine.

profile K_s distribution (Figure 10). The optimization was centered on the position below the vine, where Areas 3 and 4 represent wet and dry areas, respectively (Figure 2). An average of the two areas was compared to MLs located at the same position at random distances from the drippers (Figure 10, 4 July). For the validation period, the wet and dry areas were measured separately for the position underneath the vine, allowing for direct comparison (Figure 10, 23 July). The K_s distribution did not seem to affect simulations for the wet surfaces (Areas 2 and 3) very much over the period before noon. Over the second half of the day, however, simulations for Areas 2 and 3 differed by as much as 100%. Simulated peak E values in the areas further away from the dripper, Areas 1 and 4, varied between 0.2 and 0.4 mm/h. While variability in soil properties explained some of the variability in ML measurements, it appeared that modeled results overestimated E in the dry areas below the vine. When Area 4 was divided into three sections of 0.1 m (Figure 11), a strong decline in E with distance from wetted area (Area 3, 0 m) was observed. Compared to that at 0 m, E decreased to 81%, 45%, and 2% at distances of 0–0.1, 0.1–0.2, and 0.2–0.3 m, respectively. The results from the drier MLs were equivalent to simulated evaporation originating from areas between 0.1 and 0.3 m away from the wetted surface.

4. Discussion

The field conditions shown in Figure 3 are typical for summer in the central Negev [*Bruins*, 2012]. The winds in the afternoon were caused by the so-called sea-breeze effect as a result of relative proximity to the Mediterranean Sea [*Breckle et al.*, 2008]. As the canopy was fully grown in July and the atmospheric conditions showed little variability from day to day, ET was mostly a function of irrigation. This resulted in very similar conditions for the two IOPs, as evident by comparing both hourly ET and E_{pot} for 4 and 23 July (Figures 4 and 7). Similar results were found for Cabernet Sauvignon [*Pellegrino*, 1987] and Tempranillo [*Intrigliolo et al.*, 2012; *Picón-Toro et al.*, 2012] vineyards, where ET showed little variability starting shortly before veraison until harvest.

Variability in below canopy E_{pot} could largely be explained by canopy shading effects which changed with distance from the vine-row and time of day. This is consistent with findings by *Ham and Kluitenberg* [1993], who concluded that R_S could be used to explain most of the diurnal and positional variation in the soil energy balance beneath a soybean crop. While the shading effect on E_{pot} was also visible for E, measurements taken from the same position relative to the vine-row showed large irregularity. Discrepancies were as much as a factor of 6 between wetter and drier samples, each directly underneath the vine but at different distances from drippers. Similar variability was reported by *Zhang et al.* [2011] who found that daily values of E in a Merlot vineyard depended more on soil water content than on R_S or vapor pressure deficit. A more pronounced effect of E_{pot} on wetter areas was also observed by *Yunusa et al.* [2004], who reported distinct spatial patterns in daily E in a Sultana vineyard on days with rainfall, where under-vine E was lower than the positions 1 m away, but higher than midrow positions. They observed a similar but less pronounced spatial pattern on days with irrigation, while on dry days the differences between positions were negligible but the variability in the measurements was large, averaging 0.4 mm/d with standard errors of up to 4 mm/d. Both *Zhang et al.* [2011] and *Yunusa et al.* [2004] looked at spatial variability in daily E in vineyards with an east-west orientation where diurnal patterns in shading tend to be less variable. Two studies [*Heilman et al.*, 1994; *Holland et al.*, 2013] conducted in vineyards with a north-south orientation focused on diurnal patterns but did not include spatial variability. They reported a similar diurnal pattern for E, which increased sharply in the morning, peaked in the afternoon, and continued for 1 or 2 h after sunset. No studies were found reporting both diurnal and spatial patterns of E. While E_{pot} and ET were relatively similar for the two IOPs in the current study, total E differed by 100%, resulting in estimated ratios of E/ET of 0.08 and

0.17, respectively. Keeping in mind the high variability in E between individual samples this difference is not that surprising. However, both values are relatively small compared to fractions found in the literature [*Kool et al.*, 2014]. This is likely due to the relatively small wetted surface fraction that is typical for deficit drip-irrigated systems. Larger fractions may occur at the beginning of the season when the canopy is just starting to develop.

Optimization of root water uptake parameters using E from wet areas proved to be the most effective as both modeled and measured E from wet areas were more uniform compared to drier areas. The variable BCs in the model require transient values for E_{pot} in order to allow long-term simulations. While micropan measurements provided spatial and diurnal E_{pot}, these data were only applicable to the short IOPs. To allow continuous estimates of E_{pot} for the entire modeled period, R_s in the ET_0 computations was replaced with below canopy R_s for each position, assuming that R_{S_below} is largely responsible for positional differences in the energy balance [*Ham and Kluitenberg*, 1993]. Given the difference in measurement technique: the micropan is an in situ measurement with a free water surface, while ET_0 is calculated from weather data gathered nearby, below canopy ET_0 and micropan measurements correlated surprisingly well. Small differences between them can be attributed to variations in onset of shading, i.e., the micropans covered a larger area than the pyranometers and therefore shade reached the pans first. The use of above canopy RH, T_h, and u for computing below canopy ET_0 may have added uncertainty to ET_0 estimates [*McVicar et al.*, 2012], though the wide row spacing and narrow canopy likely minimized these discrepancies. The relatively good agreement indicates that using ET_0 with below canopy R_S is a viable option to estimate below canopy E_{pot}, although more general use would require validation for other environments. The calculated K_{cb} of 0.4 seemed reasonable; other studies reported K_{cb} values of 0.4 [*Allen et al.*, 1998], 0.43 [*Poblete-Echeverría et al.*, 2012], and 0.46 [*Carrasco-Benavides et al.*, 2012] for wine vineyards between veraison and harvest or stage III.

The HYDRUS (2-D/3-D) results compared well with ET data, particularly on nonirrigated days. It appears that after irrigation, it took until the next day for the ET to recover to its nonstressed high. The model is unable to account for this since root water uptake in HYDRUS is determined purely by water availability, while lag in recovery is likely caused by additional plant physiological responses [*Galmés et al.*, 2007]. This caused an overestimation in modeled ET on days with irrigation, and a slight underestimation of ET on the following days. The major concern of this study is quantification of E and not ET. That said, the independently measurable ET allowed preliminary evaluation of the model. Some consideration of possible contribution to ET estimation using the modified model is possible. In the case of a drip-irrigated arid vineyard in the current study, ET was largely dictated by available water (irrigation), making the improvements in ET due to the more accurate assessment of E marginal. Cumulative ET estimation likely was improved with the more accurate assessment of E, but to be valid on a daily or hourly base, more detailed modeling of plant processes is required. The contribution of the improved E estimation would possibly be more significant in environments where water is less limiting.

The HYDRUS (2-D/3-D) results were well correlated with measured E from the wet area. The drier areas were much more variable and therefore more difficult to compare. Soil properties are known to cause large variability in vineyard yield [*Bellvert et al.*, 2012; *Kerridge et al.*, 2013]. Simulating a range of possible K_s distributions was therefore very helpful to identify the range of variability in E that can be expected in the field because of natural variations. The model showed distinct differences between wet and dry areas, with an abrupt decline in E at 0.2 m compared to 0.1 m away from the dripper. These abrupt changes made it difficult to obtain representative ML measurements for the transient zone from wet to dry. Likewise, a very fine mesh was required to model these abrupt changes in HYDRUS (2-D/3-D). A fine vertical discretization close to the surface proved to be particularly important to acquire reasonable values for E [*Vanderborght et al.*, 2005]. A limitation of HYDRUS (2-D/3-D) is that heat and water fluxes are not fully coupled, neglecting water vapor fluxes [*Saito et al.*, 2006]. Since the van Genuchten-Mualem hydraulic functions may be inaccurate in very dry soils, the use of their model could be an additional source of error if applied under particularly dry conditions. In such cases, modified functions, for example *Fayer and Simmons* [1995], which allow the soil to become air dry, could improve prediction of late stage E. In spite of this, the results from this study indicate that HYDRUS (2-D/3-D) can derive E fluxes, including consideration of spatial variability, as determined by soil hydraulic properties and soil water content. The model can therefore potentially be used to evaluate E under alternative conditions or management strategies. This includes operational parameters such as drip

emitter distance, mulching, emitter depth, and irrigation scheduling. The ability of the model to simulate solute transport also poses opportunities to study effects of E on soil salinity.

5. Conclusions

The objectives of this study were to quantify E and to evaluate HYDRUS (2-D/3-D) simulation of below canopy E while considering variability in time and space. In a drip-irrigated vineyard, it was found that below canopy E_{pot} and E are highly variable both diurnally and with distance from the vine-row. While the magnitude of E was mostly determined by water content, diurnal patterns depended strongly on canopy shading. Large reduction in E_{pot} was observed directly under the vine at noon. HYDRUS (2-D/3-D) successfully simulated the magnitude and diurnal patterns of E including spatial variability due to uneven water content and soil saturated hydraulic conductivity and therefore should prove useful in simulating E under different conditions or management scenarios.

References

Agam, N., S. R. Evett, J. A. Tolk, W. P. Kustas, P. D. Colaizzi, J. G. Alfieri, L. G. Mckee, K. S. Copeland, T. A. Howell, and J. L. Chavez (2012), Evaporative loss from irrigated interrows in a highly advective semi-arid agricultural area, *Adv. Water Resour.*, *50*, 20–30, doi:10.1016/j.advwatres.2012.07.010.

Allen, R. G., L. S. Pereira, D. Raes, and M. Smith (1998), *Crop Evapotranspiration—Guidelines for Computing Crop Water Requirements*, Food and Agric. Organ. of the U. N., Rome.

Basile, B., J. Girona, M. H. Behboudian, M. Mata, J. Rosello, M. Ferré, and J. Marsal (2012), Responses of "Chardonnay" to deficit irrigation applied at different phenological stages: Vine growth, must composition, and wine quality, *Irrig. Sci.*, *30*(5), 397–406, doi:10.1007/s00271-012-0353-1.

Bellvert, J., J. Marsal, M. Mata, and J. Girona (2012), Identifying irrigation zones across a 7.5-ha "Pinot noir" vineyard based on the variability of vine water status and multispectral images, *Irrig. Sci.*, *30*(6), 499–509, doi:10.1007/s00271-012-0380-y.

Boast, C. W., and T. M. Robertson (1982), A micro-lysimeter method for determining evaporation from bare soil: Description and laboratory evaluation, *Soil Sci. Soc. Am. J.*, *46*, 689–696.

Breckle, S.-W., A. Yair, and M. Veste (2008), *Arid Dune Ecosystems: The Nizzana Sands in the Negev Desert, Ecological Studies Series*, vol. 200, Springer, Berlin.

Bruins, H. J. (2012), Ancient desert agriculture in the Negev and climate-zone boundary changes during average, wet and drought years, *J. Arid Environ.*, *86*, 28–42, doi:10.1016/j.jaridenv.2012.01.015.

Bufon, V. B., R. J. Lascano, C. Bednarz, J. D. Booker, and D. C. Gitz (2012), Soil water content on drip irrigated cotton: Comparison of measured and simulated values obtained with the Hydrus 2-D model, *Irrig. Sci.*, *30*, 259–273, doi:10.1007/s00271-011-0279-z.

Cammalleri, C., M. C. Anderson, G. Ciraolo, G. D'Urso, W. P. Kustas, G. La Loggia, and M. Minacapilli (2010), The impact of in-canopy wind profile formulations on heat flux estimation in an open orchard using the remote sensing-based two-source model, *Hydrol. Earth Syst. Sci.*, *14*(12), 2643–2659, doi:10.5194/hess-14–2643-2010.

Carrasco-Benavides, M., S. Ortega-Farías, L. O. Lagos, J. Kleissl, L. Morales, C. Poblete-Echeverría, and R. G. Allen (2012), Crop coefficients and actual evapotranspiration of a drip-irrigated Merlot vineyard using multispectral satellite images, *Irrig. Sci.*, *30*(6), 485–497, doi:10.1007/s00271-012-0379-4.

Colaizzi, P. D., S. A. O'Shaughnessy, P. H. Gowda, S. R. Evett, T. A. Howell, W. P. Kustas, and M. C. Anderson (2010), Radiometer footprint model to estimate sunlit and shaded components for row crops, *Agron. J.*, *102*(3), 942–955, doi:10.2134/agronj2009.0393.

Deb, S. K., M. K. Shukla, and J. G. Mexal (2013), Evaluation of spatial and temporal root water uptake patterns of a flood-irrigated pecan tree using the HYDRUS (2D/3D) model, *J. Irrig. Drain. Eng.*, *139*, 599–611, doi:10.1061/(ASCE)IR.1943–4774.0000611.

Evett, S. R., A. W. Warrick, and A. D. Matthias (1995), Wall material and capping effects on microlysimeter temperatures and evaporation, *Soil Sci. Soc. Am. J.*, *59*(2), 329–336.

Fayer, M. J., and C. S. Simmons (1995), Modified soil water retention functions for all matric suctions, *Water Resour. Res.*, *31*(5), 1233–1238, doi:10.1029/95WR00173.

Feddes, R. A., P. J. Kowalik, and H. Zaradny (1978), *Simulation of Field Water Use and Crop Yield*, John Wiley, N. Y.

Ferreira, M. I., J. Silvestre, N. Conceição, and A. C. Malheiro (2012), Crop and stress coefficients in rainfed and deficit irrigation vineyards using sap flow techniques, *Irrig. Sci.*, *30*(5), 433–447, doi:10.1007/s00271-012-0352-2.

Galmés, J., H. Medrano, and J. Flexas (2007), Photosynthetic limitations in response to water stress and recovery in Mediterranean plants with different growth forms, *New Phytol.*, *175*(1), 81–93, doi:10.1111/j.1469-8137.2007.02087.x.

Goring, D. G., and V. I. Nikora (2002), Despiking acoustic Doppler velocimeter data, *J. Hydraul. Eng.*, *128*, 117–126.

Ham, J. M., and G. J. Kluitenberg (1993), Positional variation in the soil energy balance beneath a row-crop canopy, *Agric. For. Meteorol.*, *63*, 73–92.

Ham, J. M., J. L. Heilman, and R. J. Lascano (1991), Soil and canopy energy balances of a row crop at partial cover, *Agron. J.*, *83*(4), 744–753.

Heilman, J. L., K. McInnes, M. Savage, R. Gesch, and R. J. Lascano (1994), Soil and canopy energy balances in a west Texas vineyard, *Agric. For. Meteorol.*, *71*, 99–114, doi:10.1016/0168-1923(94)90102-3.

Hinnell, A. C., N. Lazarovitch, A. Furman, M. Poulton, and A. W. Warrick (2010), Neuro-Drip: Estimation of subsurface wetting patterns for drip irrigation using neural networks, *Irrig. Sci.*, *28*(6), 535–544, doi:10.1007/s00271-010-0214-8.

Holland, S., J. L. Heitman, A. Howard, T. J. Sauer, W. Giese, A. Ben-Gal, N. Agam, D. Kool, and J. Havlin (2013), Micro-Bowen ratio system for measuring evapotranspiration in a vineyard interrow, *Agric. For. Meteorol.*, *177*, 93–100, doi:10.1016/j.agrformet.2013.04.009.

Horton, R. (1989), Canopy shading effects on soil heat and water flow, *Soil Sci. Soc. Am. J.*, *53*, 669–679.

Horton, R., O. Aguirre-Luna, and P. J. Wierenga (1984), Soil temperature in a row crop with incomplete surface cover, *Soil Sci. Soc. Am. J.*, *48*, 1225–1232.

Intrigliolo, D. S., D. Pérez, D. Risco, A. Yeves, and J. R. Castel (2012), Yield components and grape composition responses to seasonal water deficits in Tempranillo grapevines, *Irrig. Sci.*, *30*(5), 339–349, doi:10.1007/s00271-012-0354-0.

Jarvis, N. J. (1989), A simple empirical model of root water uptake, *J. Hydrol.*, *107*(1–4), 57–72, doi:10.1016/0022-1694(89)90050-4.

Kandelous, M. M., J. Šimůnek, M. T. van Genuchten, and K. Malek (2011), Soil water content distributions between two emitters of a subsurface drip irrigation system, *Soil Sci. Soc. Am. J.*, *75*(2), 488, doi:10.2136/sssaj2010.0181.

Kerridge, B. L., J. W. Hornbuckle, E. W. Christen, and R. D. Faulkner (2013), Using soil surface temperature to assess soil evaporation in a drip irrigated vineyard, *Agric. Water Manage.*, *116*, 128–141, doi:10.1016/j.agwat.2012.07.001.

Kool, D., N. Agam, N. Lazarovitch, J. L. Heitman, T. J. Sauer, and A. Ben-Gal (2014), A review of approaches for evapotranspiration partitioning, *Agric. For. Meteorol.*, *184*, 56–70, doi:10.1016/j.agrformet.2013.09.003.

Kumar, R., V. Shankar, and M. K. Jat (2013), Efficacy of nonlinear root water uptake model for a multilayer crop root zone, *J. Irrig. Drain. Eng.*, *139*(11), 898–910, doi:10.1061/(ASCE)IR.1943-4774.0000626.

Kumar, R., V. Shankar, and M. K. Jat (2014), Evaluation of nonlinear root uptake model for uniform root zone vis-à-vis multilayer root zone, *J. Irrig. Drain. Eng.*, *140*(2), 04013010, doi:10.1061/(ASCE)IR.1943-4774.0000655.

Kustas, W. P., and N. Agam (2014), Soil evaporation, in *Encyclopedia of Natural Resources*, edited by Y. Q. Wang, CRC Press, N. Y., in press.

Lawrence, D. M., P. E. Thornton, K. W. Oleson, and G. B. Bonan (2007), The partitioning of evapotranspiration into transpiration, soil evaporation, and canopy evaporation in a GCM: Impacts on land–atmosphere interaction, *J. Hydrometeorol.*, *8*(4), 862–880, doi:10.1175/JHM596.1.

Lazarovitch, N., U. Shani, T. L. Thompson, and A. W. Warrick (2006), Soil hydraulic properties affecting discharge uniformity of gravity-fed subsurface drip irrigation systems, *J. Irrig. Drain. Eng.*, *132*(6), 531–536.

Lazarovitch, N., M. Poulton, A. Furman, and A. W. Warrick (2009), Water distribution under trickle irrigation predicted using artificial neural networks, *J. Eng. Math.*, *64*(2), 207–218, doi:10.1007/s10665-009-9282-2.

Liu, H., G. Peters, and T. Foken (2001), New equations for sonic temperature variance and buoyancy heat flux with an omnidirectional sonic anemometer, *Boundary Layer Meteorol.*, *100*, 459–468.

Massman, W. J. (2000), A simple method for estimating frequency response corrections for eddy covariance systems, *Agric. For. Meteorol.*, *104*(3), 185–198, doi:10.1016/S0168-1923(00)00164-7.

Massman, W. J., and J. M. Ham (1994), An evaluation of a surface energy balance method for partitioning ET data into plant and soil components for a surface with partial canopy cover, *Agric. For. Meteorol.*, *67*(3–4), 253–267, doi:10.1016/0168–1923(94)90006-X.

McVicar, T. R., et al. (2012), Global review and synthesis of trends in observed terrestrial near-surface wind speeds: Implications for evaporation, *J. Hydrol.*, *416–417*, 182–205, doi:10.1016/j.jhydrol.2011.10.024.

Mualem, Y. (1976), A new model for predicting the hydraulic conductivity of unsaturated porous media, *Water Resour. Res.*, *12*(3), 513–522.

Nash, J. E., and J. V. Sutcliffe (1970), River flow forecasting through conceptual models part I—A discussion of principles, *J. Hydrol.*, *10*, 282–290.

Netzer, Y., C. Yao, M. Shenker, B.-A. Bravdo, and A. Schwartz (2009), Water use and the development of seasonal crop coefficients for Superior Seedless grapevines trained to an open-gable trellis system, *Irrig. Sci.*, *27*(2), 109–120, doi:10.1007/s00271-008-0124-1.

Newman, B. D., B. P. Wilcox, S. R. Archer, D. D. Breshears, C. N. Dahm, C. J. Duffy, N. G. McDowell, F. M. Phillips, B. R. Scanlon, and E. R. Vivoni (2006), Ecohydrology of water-limited environments: A scientific vision, *Water Resour. Res.*, *42*, W06302, doi:10.1029/2005WR004141.

Ortega-Farías, S., E. Fereres, and V. O. Sadras (2012), Special issue on water management in grapevines, *Irrig. Sci.*, *30*(5), 335–337, doi:10.1007/s00271-012-0356-y.

Pellegrino, A. (1987), *Water Relations of Vitis vinifera L. c.v. "Cabernet Sauvignon,"* 61 pp., Univ. of Arizona, Tucson.

Peñuelas, J., T. Rutishauser, and I. Filella (2009), Phenology feedbacks on climate change, *Science*, *324*, 887–888, doi:10.1126/science.1173004.

Picón-Toro, J., V. González-Dugo, D. Uriarte, L. A. Mancha, and L. Testi (2012), Effects of canopy size and water stress over the crop coefficient of a "Tempranillo" vineyard in south-western Spain, *Irrig. Sci.*, *30*(5), 419–432, doi:10.1007/s00271-012-0351-3.

Pieri, P. (2010), Modelling radiative balance in a row-crop canopy: Row–soil surface net radiation partition, *Ecol. Modell.*, *221*(5), 791–801, doi:10.1016/j.ecolmodel.2009.11.019.

Poblete-Echeverría, C., S. Ortega-Farías, M. Zuñiga, and S. Fuentes (2012), Evaluation of compensated heat-pulse velocity method to determine vine transpiration using combined measurements of eddy covariance system and microlysimeters, *Agric. Water Manage.*, *109*, 11–19, doi:10.1016/j.agwat.2012.01.019.

Saito, H., J. Šimůnek, and B. P. Mohanty (2006), Numerical analysis of coupled water, vapor, and heat transport in the vadose zone, *Vadose Zone J.*, *5*(2), 784–800, doi:10.2136/vzj2006.0007.

Sauer, T. J. (2002), Heat flux density, in *Methods of Soil Analysis—Part 1, Physical and Mineralogical Methods*, edited by J. D. Dane and G. C. Topp, pp. 1233–1248, Am. Soc. of Agron., Madison, Wis.

Schaap, M. G., F. J. Leij, and M. T. van Genuchten (2001), Rosetta: A computer program for estimating soil hydraulic parameters with hierarchical pedotransfer functions, *J. Hydrol.*, *251*(3–4), 163–176, doi:10.1016/S0022-1694(01)00466-8.

Schotanus, P., F. T. M. Nieuwstadt, and H. A. R. De Bruin (1983), Temperature measurement with a sonic anemometer and its application to heat and moisture fluxes, *Boundary Layer Meteorol.*, *26*, 81–93.

Scott, R. L., T. E. Huxman, W. L. Cable, and W. E. Emmerich (2006), Partitioning of evapotranspiration and its relation to carbon dioxide exchange in a Chihuahuan Desert shrubland, *Hydrol. Processes*, *20*, 3227–3243, doi:10.1002/hyp.6329.

Šimůnek, J., and J. W. Hopmans (2009), Modeling compensated root water and nutrient uptake, *Ecol. Modell.*, *220*(4), 505–521, doi:10.1016/j.ecolmodel.2008.11.004.

Šimůnek, J., M. T. van Genuchten, and M. Šejna (2008), Development and applications of the HYDRUS and STANMOD software packages and related codes, *Vadose Zone J.*, *7*(2), 587–600, doi:10.2136/vzj2007.0077.

Skaggs, T. H., T. J. Trout, J. Šimůnek, and P. J. Shouse (2004), Comparison of HYDRUS-2D simulations of drip irrigation with experimental observations, *J. Irrig. Drain. Eng.*, *130*(4), 304–310.

Tanner, C. B., and G. W. Thurtell (1969), Anemoclinometer measurements of Reynolds stress and heat transport in the atmospheric surface layer, *Res. and Dev. Tech Rep. ECOM 66-G22-F*, U.S. Army Electr. Command, Univ. of Wisconsin, Madison, Wis.

Taylor, S. A., and G. L. Ashcroft (1972), *Physical Edaphology—The Physics of Irrigated and Nonirrigated Soils*, W. H. Freeman, San Francisco, Calif.

Temesgen, B., R. G. Allen, and D. T. Jensen (1999), Adjusting temperature parameters to reflect well-watered conditions, *J. Irrig. Drain. Eng.*, *125*(1), 26–33.

van Genuchten, M. T. (1980), A closed-form equation for predicting the hydraulic conductivity of unsaturated soils, *Soil Sci. Soc. Am. J.*, *44*(5), 892–898.

Vanderborght, J., R. Kasteel, M. Herbst, M. Javaux, D. Thiery, M. Vanclooster, C. Mouvet, and H. Vereecken (2005), A set of analytical benchmarks to test numerical models of flow and transport in soils, *Vadose Zone J.*, *4*, 206–221.

Warrick, A. W., and N. Lazarovitch (2007), Infiltration from a strip source, *Water Resour. Res.*, *43*, W03420, doi:10.1029/2006WR004975.

Webb, E. K., G. I. Pearman, and R. Leuning (1980), Correction of flux measurements for density effects due to heat and water vapour trans-fer, *Q. J. R. Meteorol. Soc.*, *106*, 85–100, doi:10.1002/qj.49710644707.

Wilcox, B. P., D. D. Breshears, and M. S. Seyfried (2003), Rangelands, water balance on, in *Encyclopedia of Water Science*, edited by B. A. Stewart and T. A. Howell, pp. 791–794, Marcel Dekker, N. Y.

Williams, L. E., and J. E. Ayars (2005), Grapevine water use and the crop coefficient are linear functions of the shaded area measured beneath the canopy, *Agric. For. Meteorol.*, *132*(3–4), 201–211, doi:10.1016/j.agrformet.2005.07.010.

Willmott, C. (1982), Some comments on the evaluation of model performance, *Bull. Am. Meteorol. Soc.*, *1309–1313*.

Yermiyahu, U., A. Tal, A. Ben-Gal, A. Bar-Tal, J. Tarchitzky, and O. Lahav (2007), Rethinking desalinated water quality and agriculture, *Science*, *318*, 920–921.

Yunusa, I. A. M., R. R. Walker, and P. Lu (2004), Evapotranspiration components from energy balance, sapflow and microlysimetry techniques for an irrigated vineyard in inland Australia, *Agric. For. Meteorol.*, *127*(1–2), 93–107, doi:10.1016/j.agrformet.2004.07.001.

Zhang, Y., S. Kang, E. J. Ward, R. Ding, X. Zhang, and R. Zheng (2011), Evapotranspiration components determined by sap flow and micro-lysimetry techniques of a vineyard in northwest China: Dynamics and influential factors, *Agric. Water Manage.*, *98*(8), 1207–1214, doi: 10.1016/j.agwat.2011.03.006.